Response Surface based Reliability Analysis of Critical Lateral Buckling Force of Subsea Pipelines

Navid Vosooghi, Srinivas Sriramula, Ana Ivanović

School of Engineering, University of Aberdeen, Aberdeen, United Kingdom

ABSTRACT

Pipeline lateral Out-of-Straightness (OoS) can act as buckle trigger in unburied (exposed) subsea pipelines. Determining the Critical Buckling Force (CBF) of the pipeline is a computationally challenging task due to the inherent uncertainties in contributing parameters which requires utilising reliability-based approaches. This implies the need for a novel framework to develop the response surface (RS) of the CBF of a nominally straight pipeline with rogue lateral OoS which is the subject of this paper and so far, has not been fully explored in the literature. The contributing parameters in CBF are narrowed down through sensitivity studies and the trend of the CBF variation versus OoS curvature and soil lateral mobilisation is established. A novel and structured approach is taken to select the RS sample points. To calculate the CBF of a pipeline with arbitrary design variables, a kriging-based surrogate model is adopted and automated by deploying a Visual Basic Application script. The framework is fully implemented for 6" to 14" pipelines. Monte Carlo simulation is utilised to show some applications of the RS such as reliability of the buckle initiation at engineered buckling sites and susceptibility of lateral buckling considering target reliability limits.

1. INTRODUCTION

The unwanted rogue lateral OoS along the route of a nominally straight subsea pipeline is prone to develop a lateral buckle due to the axial force built up caused by operating pressure and temperature. The integrity of the pipeline can be affected by the excessive curvature (bending moments) caused by rogue lateral buckles [1]. In addition, reliability of the buckle initiation at the engineered buckling sites such as sleepers or pipeline engineered curves (between straight sections of the pipeline in a snake–lay lateral buckling mitigation design) can be adversely affected by those unwanted buckles [2,3].

There are several approaches to define the shape of a lateral OoS. This can be performed based on the laybarge worse case movements [4] which is a computationally complicated and expensive task or it can be carried out based on defining a geometrical configuration of OoS with a certain value of maximum curvature [5]. There are various analytical methods for calculation of the CBF which were

developed by Hobbs et al [11,12], Taylor et al [13] and Maltby et al [14,15]. Hobbs's work was based on developing the differential equations of a laterally buckled pipeline and therefore, initial pipeline OoS was not explicitly addressed. Taylor extended Hobbs's methodology by including the pipeline initial OoS, however, it was assumed that the shape of the OoS was following the same differential equation of the buckle which is not a very valid assumption. Maltby's analytical expression included the pipeline initial OoS and it was developed based on the classical beam-column differential equation with simple supports at the ends. This boundary condition is not reflective of the pipeline real configuration at the intersecting points of the OoS and the straight sections. This implies that existing analytical and empirical expressions cannot accurately calculate the CBF of a nominally straight pipeline as the contribution of the OoS configuration (shape) and / or soil lateral mobilisation, to which CBF is very sensitive, is disregarded. In an FE simulation, the pipeline–seabed contact frictions in axial and lateral directions need to be decoupled. The Abaqus FE package requires utilising user defined subroutines which is a very complex task [7,8,9].

The uncertainties in design parameters of CBF results in the need for deploying reliability-based assessments. However, due to lack of accuracy in analytical solutions, those assessments require execution of thousands of computationally intensive FE simulations which is not practically feasible. Therefore, a framework for developing the response surface (RS) of the CBF by performing a limited number of FE simulations is required. Development of such a framework is the main subject of this paper as it has not been fully addressed by other researchers yet. By having the RS, the CBF for a pipeline with any arbitrary design parameters can be extracted easily without the need to perform any further FE work.

In this paper, the Finite element modelling is carried out by utilising Abaqus FE software to compute the CBF of the sample points which are required for developing the RS. To avoid the use of Abaqus user–defined FRIC subroutine, the FE modelling technique outlined in [6] which benefits from a two-surface seabed is adopted here to decouple the axial and lateral pipeline-seabed interaction behaviour as required by the constitutive relationships. The methodology adopted here for defining the shape of lateral OoS is based on characterising the OoS as a single sinusoidal curve defined by its wavelength and curvature [6]. A "moment of inertia" versus "pipeline submerged weight" (I vs W_{sub}) envelope covering pipeline sizes between 6" and 14" is presented as the bases for selection of the sample points for developing the RS of CBF. Sensitivity studies are performed to narrow down the contributing parameters in CBF which are outlined in [6]. The trend of CBF variation against the maximum OoS curvature and soil lateral mobilisation is established. To develop the RS, the CBF of sample points need to be computed. The sample point selection has been carried out through a very novel and structured process addressing the range, distribution and the trend of variation of corresponding CBFs. A series of

Python scripts (Figure 4) were developed to build, run and extract the CBF values for all sample points (i.e. 1600 points). It was initially investigated if polynomial regressions can be used to address the dependency between CBF of sample points [17,18]. However, due to the high error percentages in regression method, a kriging-based surrogate model [19,20] was adopted to interpolate the CBF of a pipeline with arbitrary design variables. That was performed by computing the weighted average of CBFs of the known sample points in the neighbourhood of the design point through a two-step interpolation. In order to use the RS in reliability-based assessment which requires a large number of iterations, a Visual Basic Application (VBA) script was developed and validated to automate the kriging process. This provides a unique and comprehensive framework to demonstrate the methodology for developing the RS of CBF. The framework was utilised and the RS of CBF for pipeline sizes between 6" and 14" laid on the sandy seabeds was developed. The applications of RS were demonstrated through utilising Monte Carlo simulation (MCS) [21,22,23] in numerical examples. The required minimum sleeper height to fulfil a target failure probability of buckle initiation at sleeper was calculated and probability of buckle initiation at nominally straight sections of the pipeline (buckling susceptibility) was established.

2. CONTRIBUTING PARAMETERS IN CBF

The detailed selection process of the principal contributing parameters in the CBF, their dependencies and ranges are discussed in [6] and are briefly outlined here. The contribution parameters in CBF and their range are required to be identified as an input to FE simulation sensitivity studies. This results in identifying the parameters with minor impact or minimizing the variation range of the parameters. This facilitates limiting the number of sample points which are required for developing the RS. In specific, the resistance is provided by pipeline bending stiffness (EI) and soil lateral and axial resistance. The range of the soil axial friction coefficient (μ_{ax}) and mobilisation (Mob_{ax}) are from 0.55 to 1.2 [24] and from 0.42mm to 250mm [25], respectively. The pipeline diameter (D), submerged weight (W_{sub}) and soil submerged weight (γ) are contributing parameters to the soil lateral friction coefficient (μ_{lat}) and lateral mobilisation (Mob_{lat}). The range of the μ_{lat} studied here is assumed to be from half to two times of the best estimated value of 0.678. This provides a conservative range covering the recommendations stated in [24]. The Mob_{lat} covers values between 0.00073m to 0.06m.

The severity of the pipeline OoS in horizontal plane which acts as buckle trigger, influences the pipeline CBF. The initial configuration of pipeline can be idealised by a sinusoidal shape as a function of its wavelength (L) and maximum curvature (κ_{max}). The parameter κ_{max} can be represented by a normal distribution with mean and standard deviation values of 0 1/m and 0.0002 1/m, respectively [3]. However, to ensure the selected range of κ_{max} covers a wide range of values, the standard deviation is

increased to 0.00033 which results in an upper bound κ_{max} of 0.001 (3 x 0.00033) as 99.73% of the values lie within +/-3 standard deviations. The lower bound κ_{max} value can be considered 0.00004 1/m as it is practically impossible to lay a pipeline without such a small curvature (radius of 25 km). For κ_{max} values less than this amount, the CBF approaches infinity and is not relevant. The equivalent sinusoidal wavelength (L) considered here is 120m [3] which is the best available data in the literature. This wavelength is potentially an important parameter, and further research is required to quantify the impact of the wavelength of the OoS (in conjunction with maximum curvature) on CBF.

The parameters contributing to pipeline resistance against lateral buckling together with their range are outlined in Table 1. It is to be noted that the ranges stated in this table are valid for pipelines of sizes between 6" and 14" laid on the sandy seabeds. The pipeline size range adopted here covers the production pipelines routing between subsea wells / manifolds and receiving facilities. These pipelines contain high temperature and high pressure well fluids and are prone to lateral buckling.

Parameter	Symbol	Value / Range	Unit
Soil Axial Friction Coefficient	μ_{ax}	0.55 - 1.2	-
Soil Axial Mobilisation	Mob_{ax}	0.00042 - 0.25	m
Soil Lateral Friction Coeff.	μ_{lat}	0.339 – 1.356	-
Soil Lateral Mobilisation	Mob_{lat}	0.00073-0.06	m
As-Laid OoS Wavelength	L	120	m
As-Laid OoS Curvature	κ_{max}	0.00004 - 0.0010	$1/m$

Table 1. Range of Contributing Parameters in CBF (Resistance)

To address the contribution of the pipeline weight (W_{sub}) and stiffness (EI) in the CBF, a moment of inertia (I) versus W_{sub} envelope needs to be developed. The pipeline thickness is predominantly a function of the internal and external pressures and therefore can vary over a wide range. Therefore, for each of the selected pipeline diameters stated above, the standard pipe thicknesses (t) are extracted from ASME B36.10M [33], while the thicknesses which result in a positive pipeline submerged weight are selected as realistic thicknesses for that specific pipe diameter. The pipeline moment of inertia and submerged weight are dependant parameters as both are functions of the diameter and thickness. To address this dependency, a scatter matrix including pipeline diameter (D) versus its thickness (t) was developed and then for combinations of D and t, I and W_{sub} were calculated. Through this methodology, all realistic combinations of I and W_{sub} were populated as presented in Figure 1. The $I - W_{sub}$ envelope will be utilised for developing the CBF response surface.

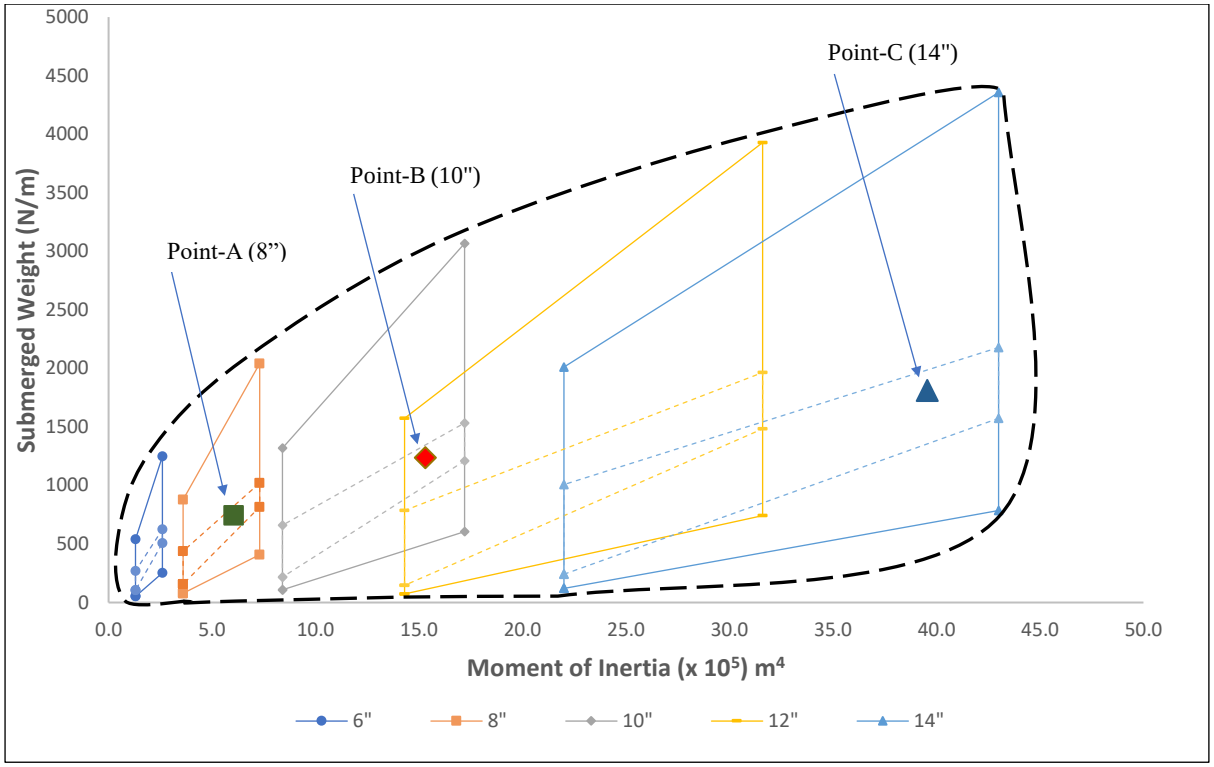

Figure 1. I vs W_{sub} envelope (for 6" to 14" pipelines)

3. FINITE ELEMENT SIMULATION

Finite element in-place model

The in-place model of the pipeline was built in the Abaqus FE software and the modelling technique developed in [6] is used here. To carry out a parametric study of the CBF and assess the sensitivity of the results to the contributing parameters outlined in Table 1, finite element simulations need to be utilised. The technique benefits from a two-surface seabed concept which can correctly capture and decouple axial and lateral pipeline-seabed interaction as required by the pipeline-seabed constitutive relationships. This technique eliminates the need for user-defined friction subroutines of Abaqus FE software which is a technically complex task. In this approach the pipeline is lowered onto the seabed to initiate normal contacts. Then initial lateral OoS profile of pipeline is obtained based on Eq. 1 for the known values of L and κ_{max}. This is applied to the pipeline as pre-defined displacements to simulate the configuration of a sinusoidal as-laid lateral OoS.

$$f(x) = \frac{\kappa_{max}}{4\pi^2}.L^2.\left[1 + sin(\frac{2\pi}{L}.x)\right], \qquad \frac{1L}{4} \le x \le \frac{5L}{4} \tag{1}$$

The pipeline-seabed interaction parameters are altered as outlined in [6] and tangential contacts (axial and lateral frictions) are activated and then, temperature is increased gradually.

A static, large-deformation geometrically non-linear analysis is deployed as the pipeline elements (nodes) experience large displacements at the stage at which the initial configuration of the lateral OoS is applied. In addition, pipeline elements at the OoS area undergo severe rotations and displacements during buckling which can be captured by large-deformation geometrically non-linear analysis only. Initially, a fully straight 6 km long pipeline section is modelled above the seabed level, considering Abaqus PIPE31 elements to model the pipeline, with the mesh size set to 1m. This is selected by performing sensitivity analysis to establish the maximum mesh size which does not affect the accuracy of the results. The pipeline is placed 1m above the seabed and all degrees of freedom are set to zero. The seabed rigid surfaces are moved up to the pipeline level to initiate the normal contact with the pipeline. This is performed by applying pre-defined displacements to the reference point of the seabed surfaces. The pipeline self-weight is applied and pipeline boundary conditions are modified to reflect the on-seabed condition of a straight pipeline (Figure 2).

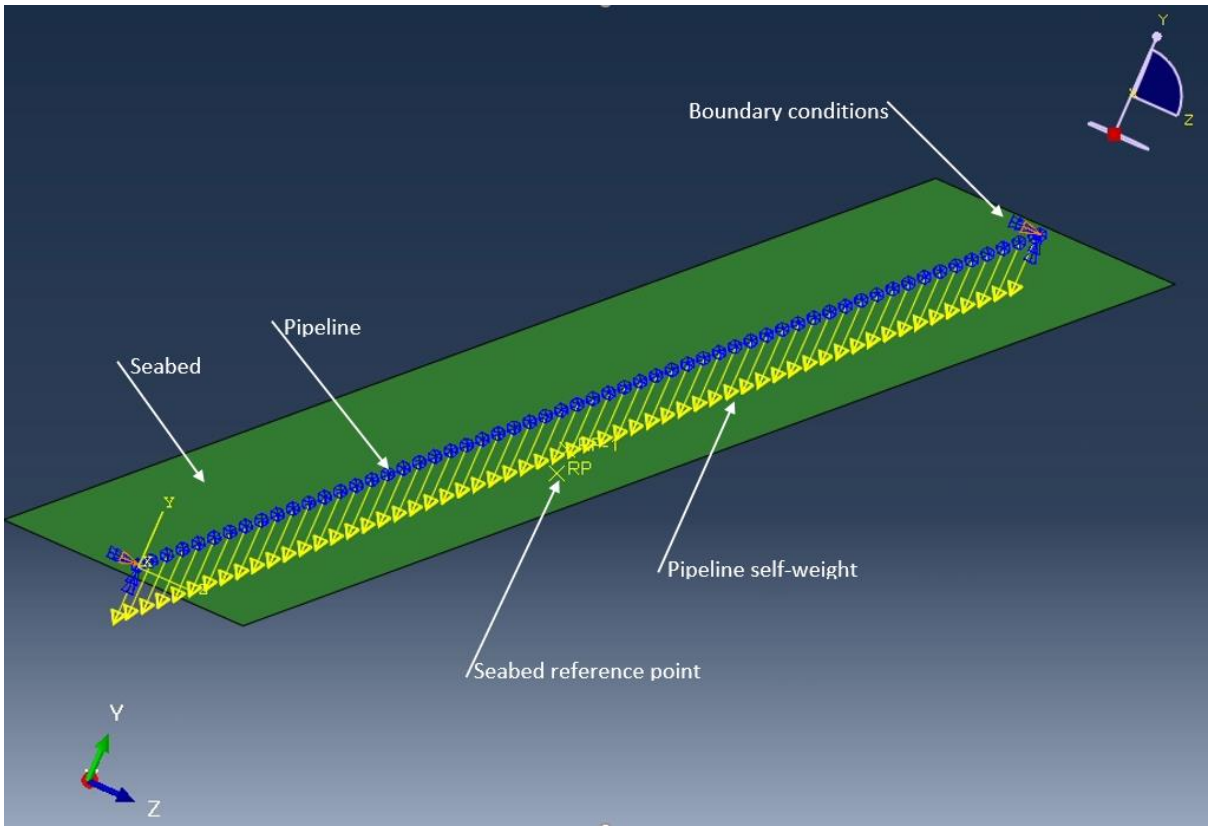

Figure 2. Abaqus Screenshot - On-Seabed Configuration (before imposing OoS)

The pipeline initial lateral OoS profile is applied as pre-defined displacements to form a sinusoidal as-laid configuration. This will introduce an imperfection to initiate the buckling in the later stages of the simulation. The pipeline end boundary conditions are set to fixed to allow accumulation of the compressive axial force once the pressure and temperature are applied.

A python script is used to monitor pipeline effective axial force (EAF) at the crown of the OoS and to specify a point at which a sharp drop in EAF is observed. This EAF is considered as the critical buckling force. An Abaqus model screenshot of the pipeline configuration at initiation of a rogue lateral buckle is shown in Figure 3.

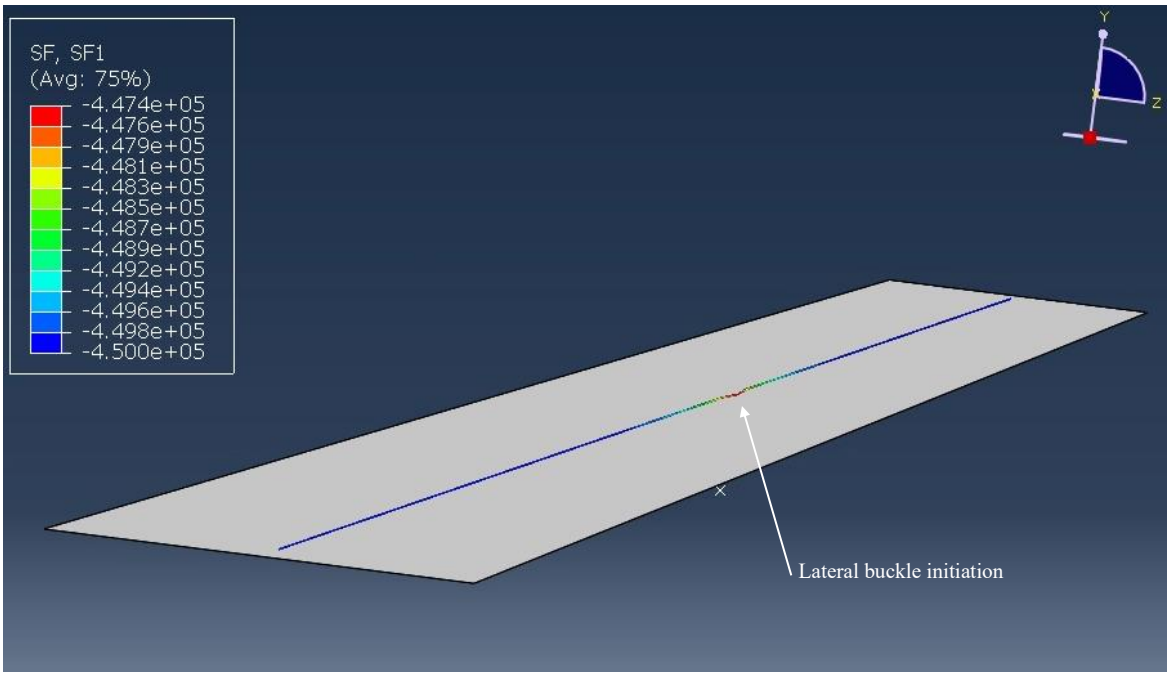

Figure 3. Abaqus Model Screenshot Showing a Rogue Lateral Buckle at Initiation

A global buckling design is acceptable provided all the stress values remain below the yield stress [34]. In addition, all the FE simulation results showed that the pipeline Von-Mises stress remained well under the yield stress at the point of the buckle initiation. Therefore, elastic material properties were considered for the pipeline. As the intention of the FE simulation is to compute the CBF of the sample of the RS, the residual lay tension is not required to be applied as it cancels in the limit state functions. This is further expanded in Section 6. In addition, it should be noted that the CBF is not a function of the residual lay tension as pipeline buckles after reaching the CBF regardless of the loading path (history of pressure and temperature increase) or initial loading condition (residual lay tension). The effects of the loading path for buckling over a sleeper is outlined in [10].

Simulation Process

In a parametric study there is a need to run a large number of models to cover all variations of the contributing parameters. Therefore, it is very beneficial and time-efficient to automate the process. In this study, Python scripting is utilised for this task. The first python script produces the lateral OoS sinusoidal configurations for chosen combinations of wavelength (L) and maximum curvature (κ_{max}) values.

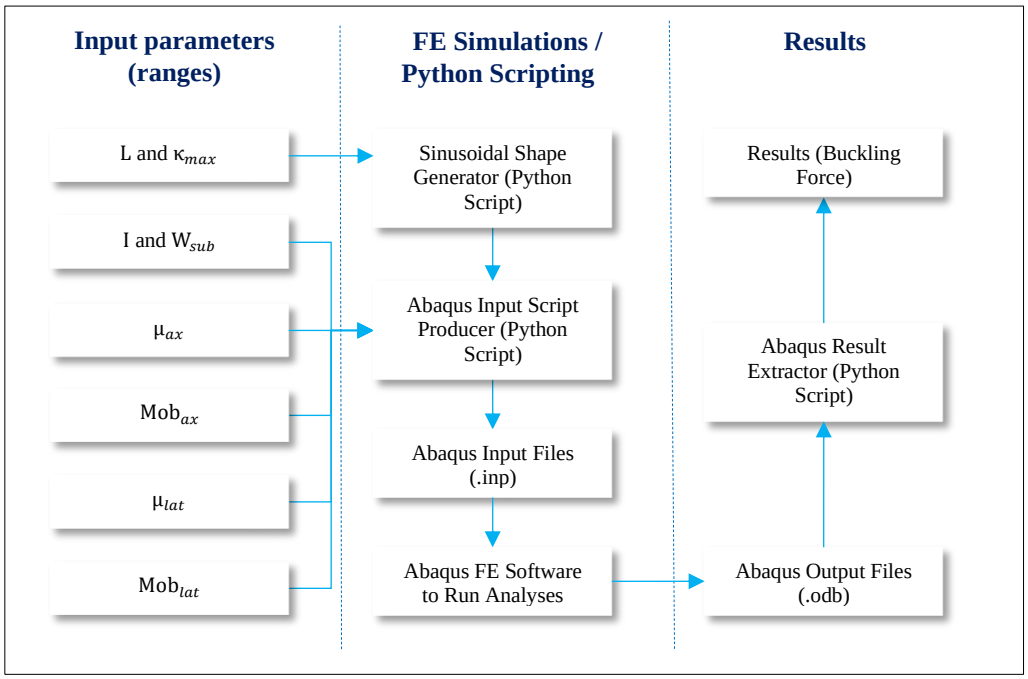

Figure 4. Numerical Simulation Flowchart

The second Python script builds Abaqus input files (.inp) which cover the full range of contributing parameters. Then, Abaqus FE software executes all input files and produces output files (.odb). The third python script is developed to extract the desired results (critical buckling force) from output files. A flow chart for the numerical simulation is outlined in Figure 4.

4. SENSITIVITY STUDY

To establish the sensitivity of the CBF to the contributing parameters, three arbitrary points of $I - W_{sub}$ envelope (Figure 1) are selected. The three points are shown in the Figure as "Point-A", "Point-B" and "Point-C" which correspond to 8", 10" and 14" size pipelines with thicknesses of 19.05mm, 25.4mm and 28.58mm, respectively. The CBF of these three points for the whole range of the parameters stated in Table 1 are calculated based on the FE modelling and simulation technique explained above. The results (Figure 5) show that the CBF values of three points are very different for the same values of as-laid OoS curvature (κ_{max}). This can easily be justified as those points represent pipelines with different values of submerged weight (W_{sub}) and moment of inertia (I). This demonstrates that κ_{max}, W_{sub} and I are among the key contributors in CBF and therefore their whole range shall be considered for developing the CBF response surface as minor variation in those parameters can result in large variation in the buckling force.

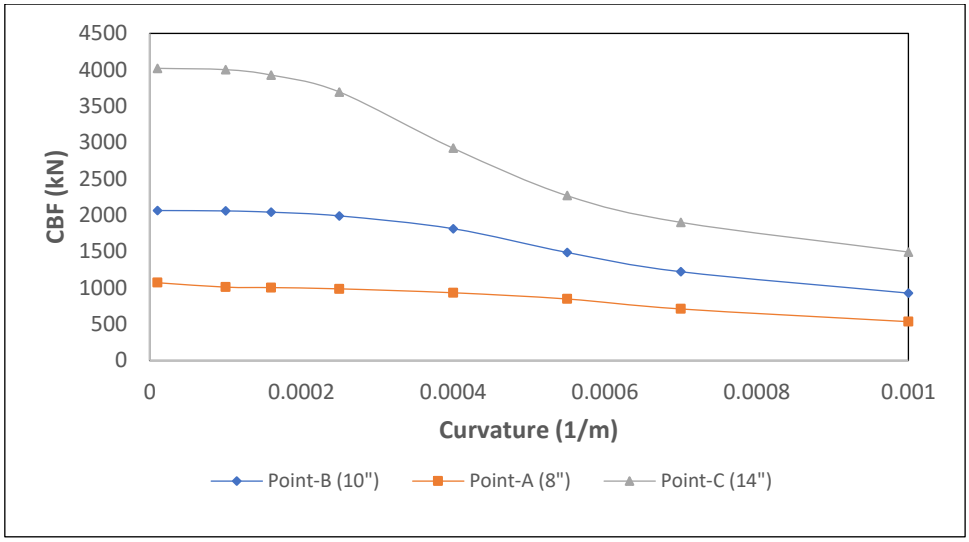

Figure 5. CBF at "Point-A", "Point-B" and "Point-C" vs Curvature

The values of CBF versus soil lateral mobilisation for "Point-A", "Point-B" and "Point-C" are plotted for a fixed value of curvature (0.00016 1/m) in Figure 6 which shows that soil lateral mobilisation is another key contributor in the CBF.

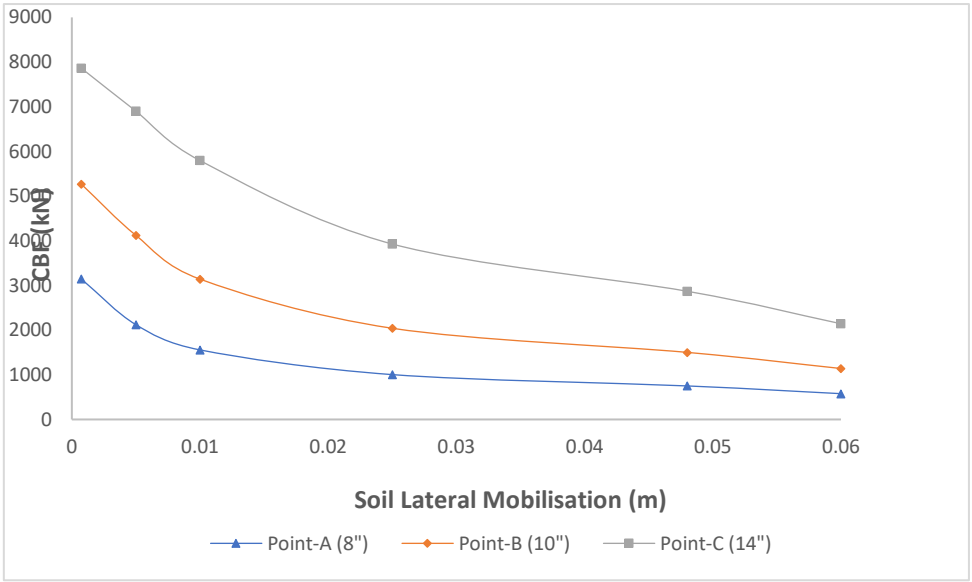

Figure 6. CBF at "Point-A", "Point-B" and "Point-C" vs Soil Lateral Mobilisation

From the sensitivity assessment and the plots presented in Figure 5 and Figure 6, the following can be concluded:

- CBF is fully dependent on the pipeline moment of inertia (I), submerged weight (W_{sub}) and lateral friction coefficient (μ_{lat});
- Mob_{lat} is a key contributor to the CBF and the higher values of Mob_{lat} result in the lower values of CBF;

- The impact of Mob_{lat} on CBF is more prominent for lower values of the κ_{max}. For higher values of κ_{max}, the CBF remains almost constant and independent of Mob_{lat};
- κ_{max} is among the key contributors in the CBF and the higher values of κ_{max} result in the lower values of CBF;
- The impact of κ_{max} on CBF is more severe for lower values of Mob_{lat}. However, for higher values of Mob_{lat} the variation of CBF against κ_{max} decreases;
- The effects of soil axial friction coefficient and mobilisation are negligible and therefore, the average values can be used as representative values.

In view of the above conclusions, the ranges of the contributing parameters outlined in Table 1 are narrowed down and presented in Table 2 and will be utilised in developing the CBF response surface. It is to be noted that the CBF is fully influenced by μ_{lat}, however, it can be incorporated by altering the W_{sub} as the soil lateral resistance is the product of μ_{lat} and W_{sub}. It should be noted that the sensitivity study was limited to three arbitrary points to provide the overall sensitivity of the CBF to the contributing parameters. However, to assure that the outcomes are fully applicable to the whole area of the $I - \mathrm{W}_{sub}$ envelope, further arbitrary points covering the boundaries of the envelope could be selected. This is beyond the scope of the paper, but the approach proposed here can be extended in required cases.

Parameter	Symbol	Value / Range	Unit
Soil Axial Friction Coefficient	μ_{ax}	0.875	-
Soil Axial Mobilisation	Mob_{ax}	0.125	m
Soil Lateral Friction Coeff.	μ_{lat}	0.339 – 1.356	-
Soil Lateral Mobilisation	Mob_{lat}	0.00073-0.06	m
As-Laid OoS Wavelength	L	120	m
As-Laid OoS Curvature	κ_{max}	0.00004 - 0.0010	$1/m$
Pipeline Stiffness and Weight	Refer to Figure 1 – Full Range		

Table 2. Range of Parameters for developing the CBF Response Surface

5. RESPONSE SURACE OF CBF

The computation of the CBF via FE simulation for a large number of the design variable (I, W_{sub}, κ_{max} and Mob_{lat}) combinations as required for reliability–based assessments is not a realistic task. In addition, due to the non-linear nature of the CBF and its sensitivity to the design variables, an explicit expression is not available. This implies the requirement for developing a transfer function called the response surface [27]. The response surface provides the means to establish a relationship between input parameters (design variables) and the output (CBF) based on rationally chosen sample points.

The CBF response surface is developed based on the $I - W_{sub}$ envelope which is presented in Figure 1. The $I - W_{sub}$ envelope of each pipeline size is the area between the upper and lower dotted lines. The soil lateral resistance (F_{lat}) is the product of μ_{lat} and W_{sub}, and the variation of μ_{lat} can be represented by altering W_{sub} accordingly. This has been considered in developing the $I - W_{sub}$ envelope by considering the pipeline weight values to 0.5 and two times of the actual W_{sub} values. The response surface is developed based on an average value of μ_{lat} which is 0.678 [6]. This covers the μ_{lat} values between 0.339 (0.678 / 2) and 1.356 (0.678 x 2). The outer dotted envelope represents the whole $I - W_{sub}$ envelope which is used for developing the CBF response surface in this paper. The CBF is computed for 40 discrete sample points representing the perimeters of the $I - W_{sub}$ envelope as shown in Figure 1. As Mob_{lat} and κ_{max} are other key contributors in CBF, all their possible combinations need to be considered in computing the CBF of each of the 40 discrete sample points stated above. The pipeline s-laid maximum curvature (κ_{max}) can be represented by a normal distribution with mean and standard deviation values of 0 1/m and 0.0002 1/m, respectively [3] as outlined in Figure 7 (dotted curve).

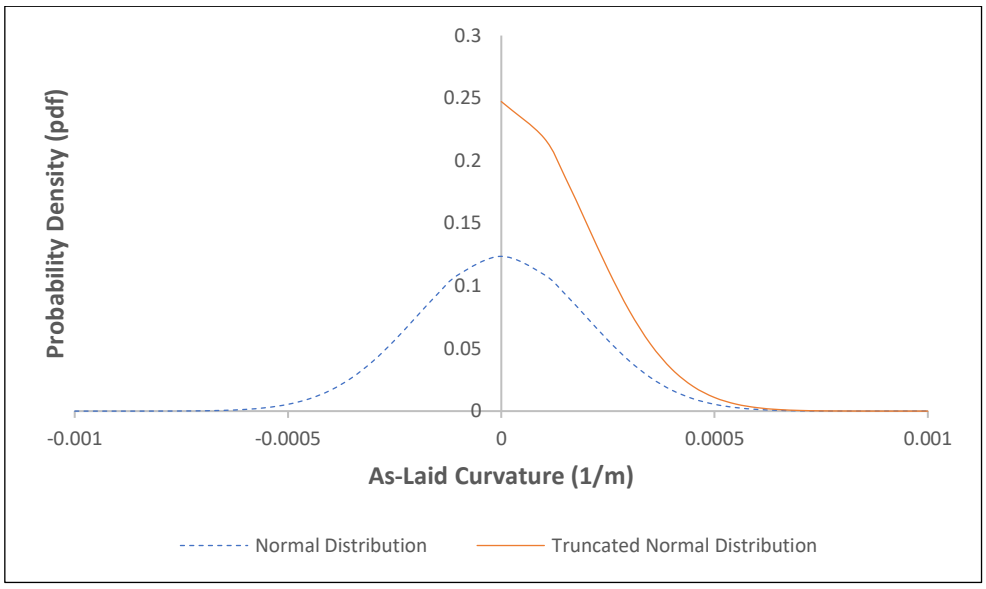

Figure 7. Probability Density Distribution of Maximum As-Laid Curvature (κ_{max})

The sign of curvature does not influence the CBF, therefore, to minimise the number of numerical simulations, there is a need to come up with a distribution which includes positive values only. A truncated normal distribution (sold line) which is derived from the original normal distribution function (pdf) fulfils this requirement by limiting the curvature values from either side to zero (mean value of normal distribution) and infinity, respectively. The general form of a truncated normal distribution density function for $a \leq x \leq b$ is:

$$(x,\mu,\sigma,a,b) = \frac{1}{\sigma}.\frac{\Phi\left(\frac{x-\mu}{\sigma}\right)}{\Phi\left(\frac{b-\mu}{\sigma}\right)-\Phi\left(\frac{a-\mu}{\sigma}\right)} \text{ and } \Phi(x) = \frac{1}{2}\left(1+erf\left(x/\sqrt{2}\right)\right) \quad (2)$$

where μ is mean value, σ is standard deviation and erf is the error function. By substituting the above boundary limit (i.e. $a = \mu$) the following is achieved:

$$\Phi\left(\frac{a-\mu}{\sigma}\right) = \frac{1}{2}\left(1+\text{erf}\left(\frac{a-\mu}{\sigma\sqrt{2}}\right)\right) = \frac{1}{2}\left(1+\text{erf}\,(0)\right) = \frac{1}{2} \quad (3)$$

$$\text{erf}(x) = \frac{2}{\sqrt{\pi}}\int_0^x e^{-t^2}dt, \text{erf}(0) = \frac{2}{\sqrt{\pi}}\int_0^0 e^{-t^2}dt = 0 \quad (4)$$

Also, based on the definition of the truncated normal distribution, if $b = \infty$ then:

$$\Phi\left(\frac{b-\mu}{\sigma}\right) = 0 \quad (5)$$

By substituting the above values in the original truncated distribution function, the density function will be simplified as following:

$$\text{f}(x,\mu,\sigma) = \frac{\frac{1}{\sqrt{2\pi}\sigma}\exp\left(-\frac{1}{2}.\left(\frac{x-\mu}{\sigma}\right)^2\right)}{0.5} \quad (6)$$

By comparison, it can be concluded that the pdf of truncated distribution function is two times of the pdf of normal distribution. The Cumulative Distribution Function (CDF) can be calculated accordingly.

The CDF of the as-laid curvatures based on truncated normal distribution is plotted in Figure 8. The solid curve represents the CDF with a standard deviation of 0.0002 1/m which is utilised here to develop the response surface. The Latin Hypercube Sampling (LHS) methodology [28, 29] is adopted here to ensure sample points are representative of the curvature distribution. For values of the CDF with an interval of 0.2 (i.e., 0.2, 0.4, 0.6, 0.8 and 1.0), corresponding curvature values (i.e., 0.4e-5, 1.0e-4, 1.6e-4, 2.5e-4 and 5.5e-4) are extracted (Figure 8) and used as discrete curvature values (curvature sample points) for developing the RS.

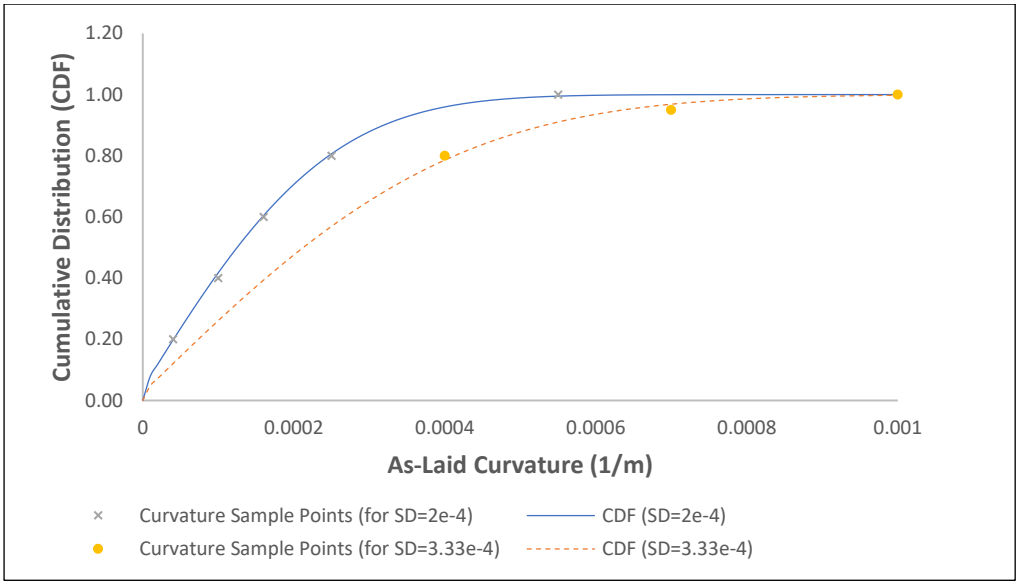

Figure 8. Probability Density Distribution of As-Laid Curvature

To ensure the distributions with wider standard deviations up to SD=3.33e-4 (dotted curve in Figure 8) are properly covered, three extra points (4e-4, 7e-4 and 1.0e-3) are added. This implies that in total eight curvature sample points are selected. The trend of CBF change versus soil lateral mobilisation is shown in Figure 6. The Mob_{lat} sample points are selected to address the gradient of CBF by having extra point in the areas where large deviations are observed. In total five Mob_{lat} sample points (i.e., 0.00073, 0.005, 0.01, 0.025, 0.06) are selected.

This implies that for each of the 40 sample points of $I - \mathrm{W}_{sub}$ envelope, there are 40 combinations of the κ_{max} (8-off) and Mob_{lat} (5-off). In total 1600 FE simulations were executed to ensure the whole range of design variables (contributing parameters) are covered. The FE simulation results were used to develop the CBF response surface. The response surface is represented by 40 planes. Each plane covers the full boundaries of $I - \mathrm{W}_{sub}$ envelope for a specific combination of κ_{max} and Mob_{lat}.

Legend in Figure 9	$\boldsymbol{\kappa_{max}}$	$\boldsymbol{Mob_{lat}}$
CBF_1st_Comb	0.00016	0.005
CBF_2nd_Comb	0.00016	0.025

Table 3. $\boldsymbol{\kappa_{max}}$ and $\boldsymbol{Mob_{lat}}$ combinations used in Figure 9

As an illustration, for the combinations outlined in Table 3, the CBF response planes are shown in Figure 9.

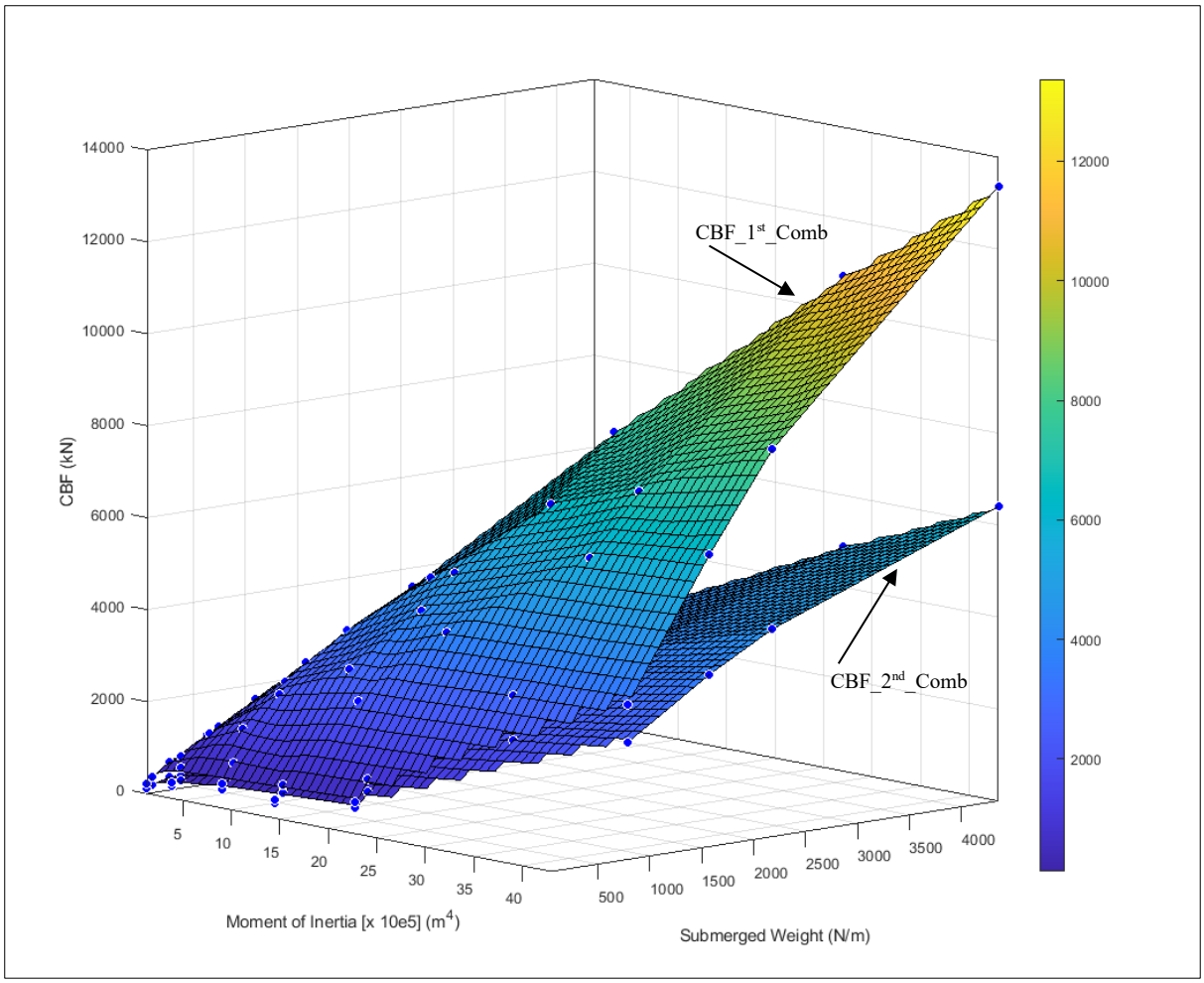

Figure 9. CBF Typical Response Planes

The polynomial response surface method which is widely used for engineering purposes [17,18] was initially investigated by performing the first, second and third-degree polynomial regressions to fit the best planes to each individual response plane. Further second order polynomial regressions were carried out to address the dependency of the CBF planes on κ_{max} and Mob_{lat}. The CBF of the pipelines with arbitrary design variables were computed by FE simulation and compared with the results from the above regression. The error percentages were very high and therefore, it was concluded that the polynomial regression is not the best approach to model the CBF response surface.

A kriging-based surrogate model [19,20] was adopted to interpolate the CBF of a pipeline with arbitrary design variables (I_d, W_{sub}_d, κ_{max}_d, Mob_{lat}_d) referred as deign point. In kriging, it is assumed that there is a spatial correlation between the model prediction and the dependencies between the CBF values formulated. This is performed by computing the weighted average of CBFs of the known sample points in the neighbourhood of a design point through a two-step interpolation:

- Four known sample points from $I - W_{sub}$ envelope (Figure 1) surrounding the design point (I_d and W_{sub}_d) are selected.

- For each of the four selected sample points, the CBFs of all 40 combinations of κ_{max}, Mob_{lat} are looked up. And then, based on the values of $\kappa_{max\_}d$ and $Mob_{lat\_}d$, a bi-linear interpolation is carried out to calculate the interpolated CBF (CBF_{κ_Mob}) corresponding to each of the selected sample points:

$$CBF_{\kappa\_Mob}(\kappa_{max\_}d, Mob_{lat\_}d) = \frac{Mob_2 - Mob_{lat\_}d}{Mob_2 - Mob_1}\left[\frac{\kappa_2 - \kappa_{max\_}d}{\kappa_2 - \kappa_1} CBF(\kappa_1, Mob_1) + \frac{\kappa_{max\_}d - \kappa_1}{\kappa_2 - \kappa_1} CBF(\kappa_2, Mob_1)\right] + \frac{Mob_{lat\_}d - Mob_1}{Mob_2 - Mob_1}\left[\frac{\kappa_2 - \kappa_{max\_}d}{\kappa_2 - \kappa_1} CBF(\kappa_1, Mob_2) + \frac{\kappa_{max\_}d - \kappa_1}{\kappa_2 - \kappa_1} CBF(\kappa_2, Mob_2)\right] \quad (7)$$

In the above expression, κ_1, κ_2, Mob_1 and Mob_2 represent the curvature and mobilisation values of the known sample points surrounding the $\kappa_{max\_}d$ and $Mob_{lat\_}d$. The $CBF(\kappa_i, Mob_j)$ represent the known values of the corresponding CBFs which are available from FE simulations.

- This is further explained in Figure 10 for a design point with design variables of: I_d =15.3e-5 m^4, $W_{sub\_}d$ =1237 Nm^{-1}, $\kappa_{max\_}d$ =0.00011 m^{-1} and Mob_{lat_d} =0.0075 m. The surface represents the CBF for all combinations of κ_{max} and Mob_{lat} belonging to one of the surrounding sample points. The interpolated value of CBF is shown as a hexagon.

- By knowing four values of CBF, an inverse distance weighing interpolation [30] is carried out and the CBF corresponding to the design point is computed. For the design point stated above, the calculated CBF is 3977 kN.

For a reliability-based assessment, a very large number of iterations are required. To address this issue, a Visual Basic Application (VBA) script was developed to automate the above explained kriging process. The VBA deploys several subroutines and functions to carry out the kriging interpolation. To validate the interpolation process and the algorithms used in the VBA script, the CBF of three arbitrary design points from $I - W_{sub}$ envelope (shown in Figure 1), were computed by FE simulation and compared with the VBA script outputs. The results for arbitrary values of κ_{max} and $Mob_{lat}$of are presented in Table 4.

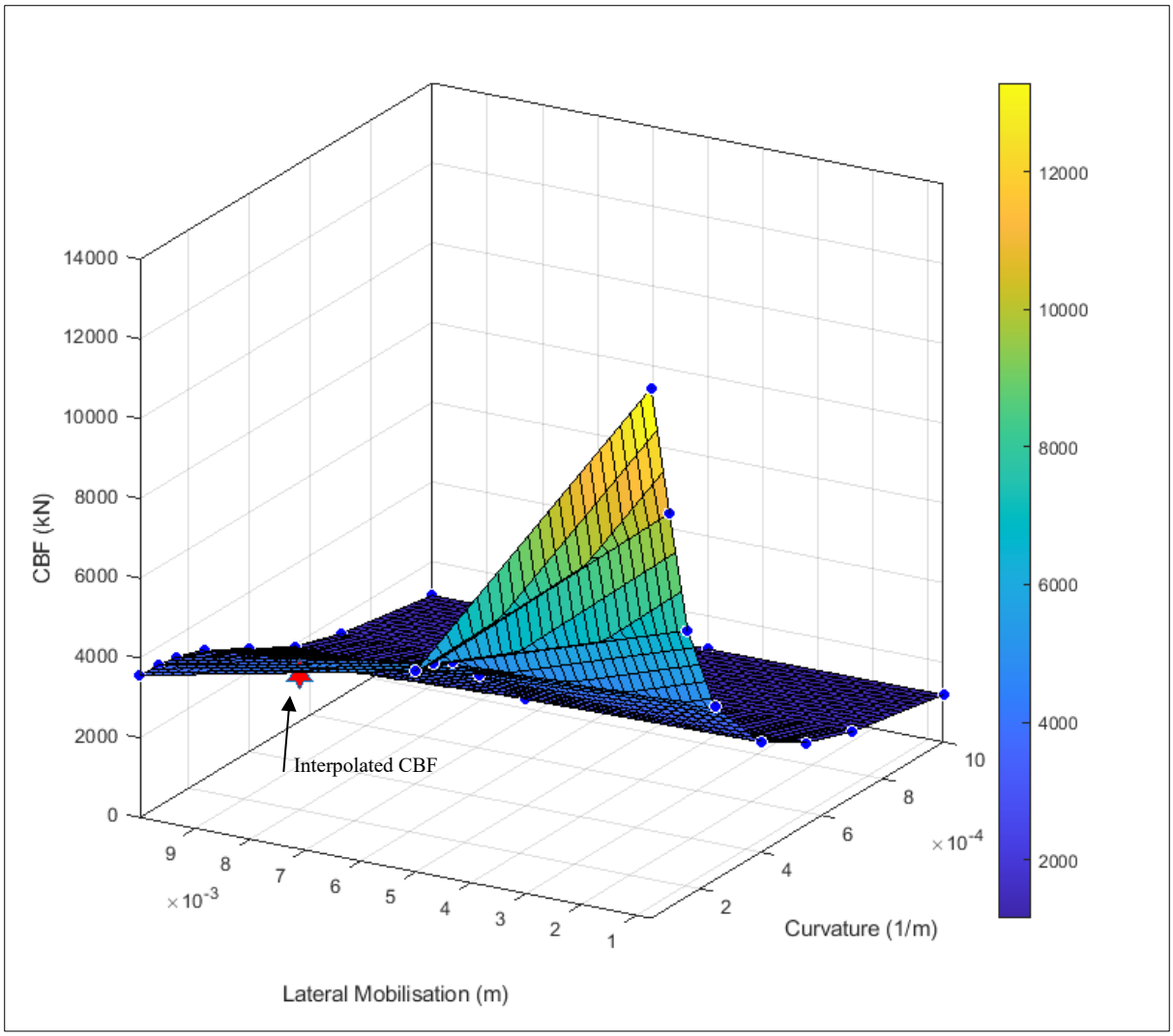

Figure 10. Illustration of Bi-Linear Interpolation (κ_{max} and Mob_{lat})

Considering the wide range of buckling force, the error levels can be treated as acceptable. Therefore, it can be concluded that the kriging methodology and VBA script are validated and can be used for further studies. It should be noted that more accuracy can be obtained by increasing the sample points in the neighbourhood of the desired design point(s).

		CBF (kN)								
		Point-A			Point-B			Point-C		
κ_{max}	Mob_{lat}	VBA Script (Interpolation)	FE Simulation	Error (%)	VBA Script (Interpolation)	FE Simulation	Error (%)	VBA Script (Interpolation)	FE Simulation	Error (%)
1.1e-4	0.0075	1816	1824	0.48	3977	3681	8.05	6856	6989	1.90
1.1e-4	0.055	679	682	0.39	1501	1392	7.78	2652	2692	1.51
3.3e-4	0.0075	1374	1442	4.72	2565	2478	3.48	3912	3780	3.49
3.3e-4	0.055	662	677	2.33	1430	1347	6.21	2436	2610	6.68
6.6e-4	0.0075	791	785	0.72	1374	1348	1.94	2107	2115	0.37
6.6e-4	0.055	587	617	4.88	1146	1196	4.23	1746	1734	0.68

Table 4. Comparison between FE Simulation and Kriging Results

The framework presented in Figure 11, outlines the methodology which is utilised in this paper for developing the RS of CBF.

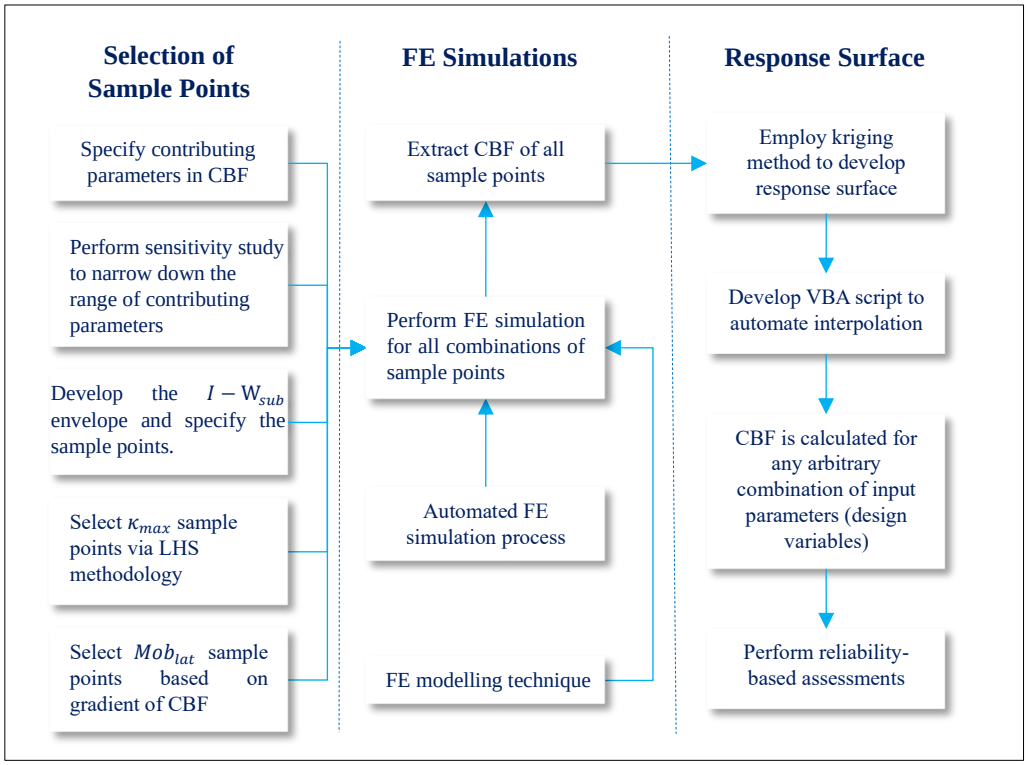

Figure 11. Framework for developing the RS of CBF

The variations in other primary variables such as pipeline diameter, thickness and Young's Modulus of steel can be incorporated by altering W_{sub} and / or I. Also, variation in the lateral friction can be addressed by altering the W_{sub}.

It should be noted that any reliability-based assessment heavily relies on robust uncertainty quantification. Therefore, careful consideration shall be given to the statistical representation of the

input parameters and their probability distributions. For example, the distribution of the OoS curvature can be extracted from the post-lay surveys of the pipelines with similar features such as cross-sectional dimensions (stiffness), water depth, and laybarge characteristics.

6. APPLICATIONS OF RS OF CBF

The RS can be used in all deterministic assessments where the CBF for a specific design point is required. The use of RS eliminates the requirement for performing the FE assessment. For example, by knowing the CBF and utilising Eq. 11, the envelope of pressure-temperature values which can cause lateral buckling can be obtained. The RS can be utilised for reliability–based assessments which is explained further below.

Monte Carlo Simulation

In a reliability-based assessment, the statistical distributions of the load effect (S) and resistance (R) are required to be known and the probability of failure (p_f) is calculated based on:

$$p_f = P(R \leq S) = P[G(R,S) \leq 0] = \int_{-\infty}^{\infty} F_R(x).f_s(x).dx \quad (8)$$

The $G(R,S)$ is called the limit state function and the probability of failure is represented by the probability of limit state violation i.e., probability of $G(R,S)$ being ≤ 0 (or probability of R being less than or equal to S). Here $F_R(x)$ and $f_s(x)$ are the CDF of R and pdf of S, respectively. In the context of this paper, the resistance (R) is the CBF of a nominally straight pipeline. In contrast, the load effect (S) can be selected to solve various engineering problems. For example, if the reliability of buckle initiation at an engineered buckling site (sleeper) is of interest, S is the buckling force at sleeper and cases at which S is greater than R, represent limit state violations (Failure). Solving the above integral - known as convolution integral - can be very difficult for real engineering problems involving several load effect and resistance parameters [16]. However, solving the convolution integral can be avoided as other techniques such as Monte Carlo simulation (MCS) are utilised to derive the reliability index [21,22,23]. In MCS, the limit state is evaluated for a large number of random variable sets (N trials) covering both R and S. The probability of failure is defined as

$$p_f = \frac{n(R-S \leq 0)}{N} \quad (9)$$

where n denotes the number of trials for which $R - S \leq 0$.

Application 1: Reliability of buckle initiation at engineered buckling site (sleeper) – Selection of Sleeper Height

The CBF at an engineered buckling site (S) needs to be less that the CBF of the adjacent nominally straight sections of the pipeline (R). The S can be assumed as a fixed (deterministic) value (S_{det}) as it is predominantly a function of the sleeper height. The problem here is to specify a sleeper height to provide a buckle initiation target failure probability of 1e-3, 1e-4 and 1e-5 corresponding to low, medium and high safety classes of DNVGL-ST-F101 [31]. The assessment is carried out for a pipeline with diameter, thickness and weight of 0.273m (10"), 0.0254m and 1237kg/m, respectively. A design pressure of 460bar and temperature of 25 °C are adopted in this example. The random design variables contributing to R and their assumed statistical distributions are outlined in Table 5. The other design variables contribution to R (i.e., E, D and t) and S (i.e., ν and E) are assumed to be fixed (deterministic).

Random Variable	Distribution	Mean	Standard Deviation
κ_{max}	Truncated Normal	0 (m^{-1})	2e-4 (m^{-1})
Mob_{lat}	Lognormal	0.01(m)	0.25 (m)
μ_{Lat}	Lognormal	0.678 (-)	0.16 (-)

Table 5. Statistical Distributions of Random Variables Contributing to *R*

The limit state function can be defined as shown in Eq. 10. The VBA script is utilised to automatically calculate the value of $Surf()$ in each iteration. Then Eq. 9 is used to calculate the probability of failure.

$$G(R,S) = Surf(I, \mathrm{W}_{sub}, \kappa_{max}, Mob_{lat}) - S_{det} \quad (10)$$

An MCS with 50,000 trials was carried out to obtain the CDF of the CBF at nominally straight sections of the pipeline (R) as shown in Figure 12. The selected number for trials is based on the sensitivity checks which showed that the results remain almost unchanged for trials equal to or greater than 50,000.

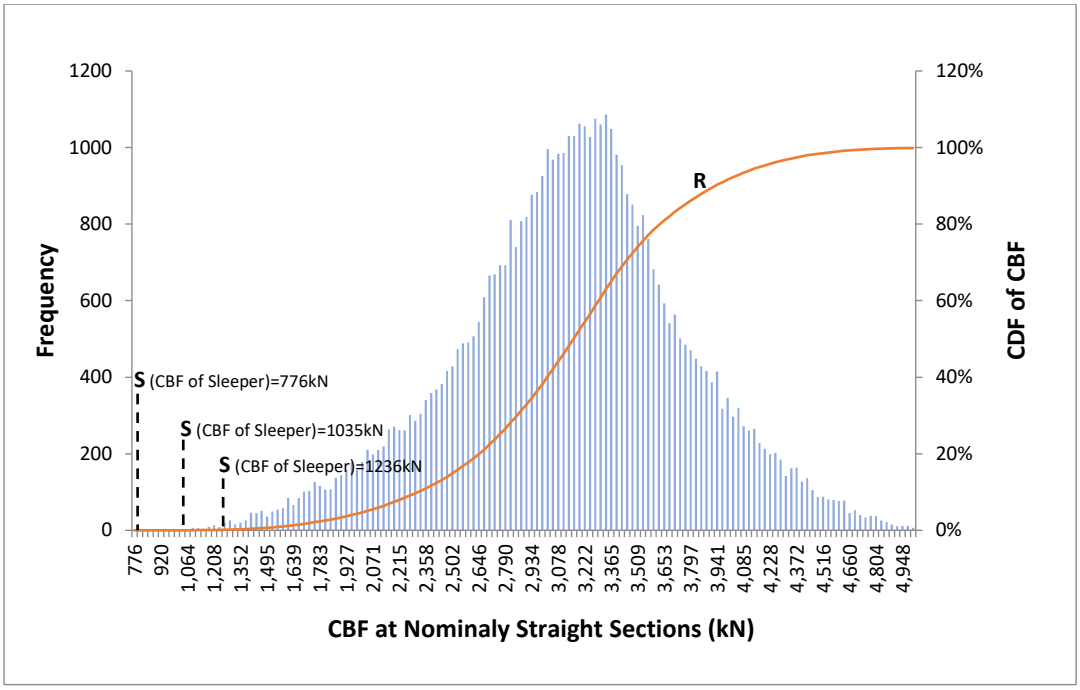

Figure 12. CDF of CBF at Nominally Straight Sections of Pipeline

The CBF at sleeper was calculated for a range of sleeper heights based on the methodology outlined in [10]. A screenshot of the Abaqus model is presented in Figure 13. In this example, pipeline lateral OoS at the sleeper is conservatively overlooked. The lateral OoS at the sleeper results in reduction in the CBF and facilitates buckling. To initiate the lateral displacement at the sleeper, a very small artificial lateral load (i.e., 2000 N) is introduced. An alternative approach to initiate the lateral displacement at the sleeper (by introducing lateral OoS) was outlined in [35,36].

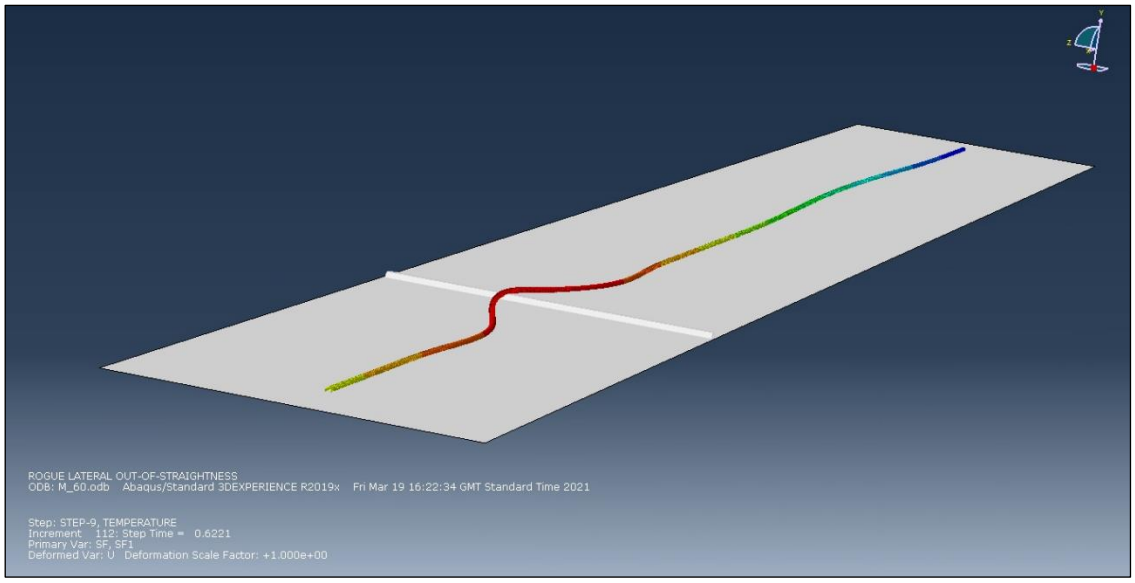

Figure 13. Abaqus Screenshot – Buckling of the pipeline at sleeper

The CBF at sleeper is extracted by utilising a python script which monitors the effective axial force (EAF) in the pipeline and defines the point at which buckle initiation occurs and a severe drop in EAF is observed. The sleeper's CBF versus sleeper height is plotted in Figure 14.

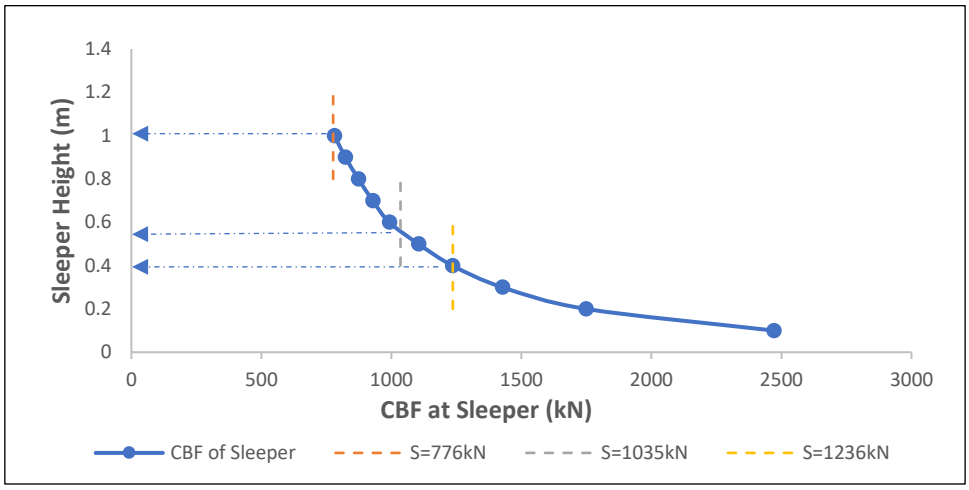

Figure 14. CBF at Sleeper vs Height

The values of S corresponding to CDFs of 1e-3, 1e-4 and 1e-5 are 1236kN, 1035kN and 776kN, respectively (Figure 12). From Figure 14, the sleeper heights to provide those values of CBF (or less) required to be greater than 0.4m, 0.55m and 1m, respectively. The target failure probability of a pipeline depends on its safety class (i.e., proximity to a manned offshore platform and fluid category). The minimum sleeper heights and the corresponding free span lengths for different locations and conditions are presented in Table 6. This shows the impact of the target failure probability on the free span length which can severely increase fatigue damage due to direct wave actions and vortex induced vibration (VIV) [32].

Condition	Location of Sleeper	Target Failure Probability	Sleeper Height (m)	Free Span Length (m)
Operating	Inside Platform 500m Zone	1e-5	1.0	90
Operating	Outside Platform 500m Zone	1e-4	0.55	60
Hydrotest	N/A	1e-5	0.4	48

Table 6. Sleeper Height and Free Span Length

Application 2: Lateral Buckling Susceptibility of a Nominally Straight Pipeline (NSP)

The effective axial force (EAF) in a pipeline is predominantly a function of the internal pressure (Δp_i), temperature (ΔT) and residual lay tension (H):

$$EAF = -\Delta p_i . A_i . (1 - 2\nu) - A_s . E . \alpha . \Delta T + H \quad (11)$$

Where A_i, ν, E, and α are internal area of the pipe, Poisson's ratio, Young's modulus and coefficient of thermal expansion of steel, respectively. The EAF can be treated as S and it should be less than the CBF of an NSP (R) to avoid buckling. The limit state function can be defined as following.

$$G(R,S) = Surf(I, W_{sub}, \kappa_{max}, Mob_{lat}) - (-\Delta p_i . A_i . (1-2\nu) - A_s . E . \alpha . \Delta T) \quad (12)$$

To demonstrate the application of the RS of the CBF for assessing the pipeline buckling susceptibility, the same pipeline (which was used in application 1) and with the same distribution of the design variables contributing to R is studied here. However, the pressure and temperature are assumed to follow the distributions outlined in Table 7. The other design variables are assumed to be fixed (deterministic).

Random Variable	Distribution	Mean	Coeff. Of Variation
Temperature (°C)	Normal	25	5%
Pressure (barg)	Normal	460	2%

Table 7. Statistical Distributions of Random Variables Contributing in *S*

By utilising the VBA script, 50,000 trials were carried out to obtain the CDF of R and pdf of S as shown in Figure 12. The Probability of Failure (p_f) is obtained using an MCS approach in accordance with Eq. 9. The p_f which in the context of this application represents probability of buckling in the NSP is 3.65%. This corresponds to a reliability of 96.35%. If the target reliability of 95% is of interest, it can be concluded that the pipeline is not prone to the buckling phenomenon.

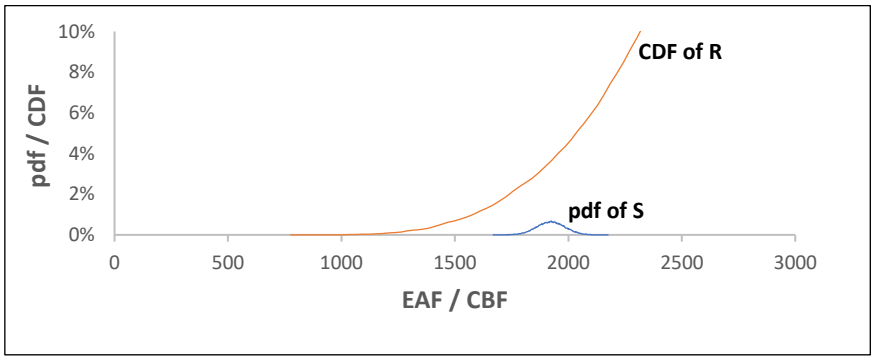

Figure 15. CDF of *R* and pdf of *S*

It should be noted that the residual lay tension (H) is not included in the above stated limit state functions (Eq. 10 and Eq. 12) as H is present in both S and R and therefore, will be balanced in the limit state function. However, the variable H can be added if different distributions of H are available for different sections of the pipeline or if deterministic values of H are of interest (e.g., to make the analysis more conservative by only adding H to S).

As a further example of other reliability-based applications of the RS of CBF, the reliability of buckle initiation at the engineered bends utilised in a snake-lay lateral mitigation method can be stated. In such a design, the pipeline is laid with several engineered curves (bends) between the straight sections to promote the pipeline to buckle at those bends. The CBF at bends (S), is predominantly a function of the bend curvature. Therefore, by knowing the target bend curvature and considering a distribution for that and utilising the RS, the distribution of S can be achieved. In this example, R is the CBF of the adjacent nominally straight sections of the pipeline which was further explained in Application 1.

7. CONCLUSIONS

The work outlined in this paper narrows down the contributing parameters in CBF of a nominally straight pipeline through sensitivity studies and the trend of the CBF variation versus OoS curvature and soil lateral mobilisation. It is concluded that CBF is fully dependent on the pipeline moment of inertia (I), submerged weight (W_{sub}), soil lateral friction coefficient (μ_{lat}), soil lateral mobilisation (Mob_{lat}) and maximum OoS curvature (κ_{max}). It was shown that the impact of Mob_{lat} on CBF is more severe for lower values of the κ_{max}. For higher values of κ_{max}, the CBF remains almost constant and independent of Mob_{lat}. It was demonstrated that the impact of κ_{max} on CBF is more severe for lower values of Mob_{lat}. However, for higher values of Mob_{lat} the variation of CBF against κ_{max} decreases. It was also concluded that the effects of soil axial friction and mobilisation are negligible.

It was observed that a truncated normal distribution function defines the maximum OoS curvature. A novel and structured approach was outlined to select the sample points which are required for developing the RS considering the range, distribution and the trend of variation of corresponding CBFs. The CBF of sample points (i.e., 1600 points) were computed by FE simulation utilising a number of Python scripts to automate the process (Figure 4). It was initially investigated whether the polynomial regression can be used to address the dependency between CBF of sample points. However, as the error percentage was very heigh, a kriging-based surrogate model was adopted instead. The process was automated by developing a Visual Basic Application (VBA) script. The VBA was validated against the FE simulation results for arbitrary design points. This resulted in a comprehensive and unique framework (Figure 11) for developing the RS of the CBF of a nominally straight pipeline with rogue lateral OoS. The framework was utilised to achieve a RS covering pipeline sizes between 6” and 14” laid on sandy seabeds. Finally, Monte Carlo simulation (MCS) was utilised to show some applications of the RS in reliability-based assessments. Truncated normal and lognormal distributions were selected for design variables of κ_{max}, Mob_{lat} and μ_{Lat}. The sleeper heights fulfilling target failure probabilities of buckle initiation, with respect to the pipeline location class for both operating and hydrotest cases, were established. Subsequently, the impact of the sleeper height on the pipeline free span length (over

the sleeper) was demonstrated. Normal distributions for pipeline pressure and temperature were selected and relevant limit state function addressing probability of buckle initiation at nominally straight sections of the pipeline was developed. Accordingly, pipeline susceptibility to lateral buckling was studied. The proposed framework for RS development and subsequent reliability analysis can also be applied to study performance and reliability of the engineered buckle initiators such as sleepers, buoyancy module segments and snake-lay configurations.

8. REFERENCES

1 J. Sun, P. Jukes, H. Shi, Thermal Expansion / Global Buckling Mitigation on HPHT Deepwater Pipelines, Sleepers or Buoyancy?, Proceedings of the Twenty-Second International Offshore and Polar Engineering Conference, 2012;

2 G. E. Harrison, M. S. Brunner, D. A. S. Bruton, King Flow lines – Thermal Expansion Design and Implementation, Offshore Technology Conference, OTC 15310, 2003;

3 I. Matheson, M. Carr, R. Peek, P. Saunders, N. Georg, Penguins Flowline Lateral Buckling Formation Analysis and Verification, Proceedings of the 23rd International Conference on Offshore Mechanics and Arctic Engineering, OMAE, 2004;

4 A. Rathbone, G. Cumming, A Holistic Design Approach for Considering Rogue Buckle Formation due to Pipelay-Induced Out-of-Straightness, Proceedings of the ASME 2010 29th International Conference on Ocean, Offshore and Arctic Engineering, OMAE 2010;

5 A. D. Rathbone, K. Tornes, G. Cumming, C. Roberts, Effect of Lateral Pipelay Imperfection on Global Buckling Design, Proceedings of the Eighteenth International Offshore and Polar Engineering Conference Vancouver, C, Canada, 2008;

6 N. Vosooghi, A. Ivanovic, S. Sriramula, Rogue Lateral buckle Initiation at Subsea Pipelines, Applied Ocean Research, 117 (2021) 102899, 2021

7 F. Yang, Y. Tian, Development of ABAQUS User Subroutine for Advanced Pipe/Soil Modelling, CEED Seminar Proceedings, 2014;

8 Z. Hong, R. Liu. Submarine Pipeline Lateral Global Buckling and Buckling Failure Critical State Discussion, Journal of Harbin Institute of Technology, 2018;

9 H. Stutz, D. Masin, A. S. Sattari, F. Wuttke, A General Approach to Model Interfaces using Existing Soil Constitutive Models Application to Hypoplasticity, Computer and Geotechnics 87 (2017) 115-127;

10 N. Vosooghi, A. Ivanovic, S. Sriramula, Contribution of Axial Soil Resistance in Buckle Initiation of the HPHT Pipelines on Sleepers, Proceedings of the ASME 2016 35th International Conference on Ocean, Offshore and Arctic Engineering, OMAE2016-54137, 2016, Korea;

11 R. E. Hobbs, In-Service Buckling of Heated Pipelines, Journal of Transportation Engineering, 110(2), 175-189, 1984;

12 R. H. Hobbs, F. Liang, Thermal Buckling of Pipelines Close to Restrains, International Conference of Offshore Mechanics and Arctic Engineering, 1989;

13 N. Taylor, A. B. Gan., Submarine Pipeline Buckling - Imperfection Studies, Thin-Walled Structures 4, 295-323, 1986;

14 T. C. Maltby, C. R. Calladine, An Investigation into Upheaval Buckling of Buried Pipelines – II Theory and Analysis of Experimental Observations, Int. J. Mech. Sci., Vo. 37, 1995;

15 H. Karampour, F. Albermani, J. Gross, On Lateral and Upheaval buckling of Subsea Pipelines, Engineering Structures 52 (2013);

16 G. Brown, M. Brunner, X. Qi, Lateral Buckling Reliability Calculation Methodology Accounting for Buckle Interaction, Offshore Technology Conference, OTC 17795, 2006;

17 C. Bucher, U. Bourgund, A fast and efficient response surface approach for structural reliability problems. Struct Saf. 7(1):57–66, 1990;

18 P. K. Das, Y. Zheng, Cumulative formation of response surface and its use in reliability analysis, Probabilistic Engineering Mechanics, 15 (4), pp.309-315, 2000;

19 I. Kaymaz, Application of kriging method to structural reliability problems, Struct Saf. 27(2):133–151, 2005;

20 J. P. C. Kleijnen, Kriging metamodeling in simulation: A review, European Journal of Operational Research, 192 (3), pp.707-716, 2009;

21 A. Naess, B. J. Leira, O. Batsevych, System reliability analysis by enhanced Monte Carlo simulation, Structural Safety, 31 (5), pp.349-355, 2009;

22 M. H. Kalos, P. A. Whitlock, Monte Carlo Methods, New York: Wiley, 2008;

23 R. E. Melchers, Structural Reliability Analysis and Prediction, Second Edition, Wiley, 2002;

24 PD 8010-2:2004, Code of Practice for Pipelines – Part 2: Subsea Pipelines;

25 DNVGL-RP-F114 Recommended Practice, Pipe-Soil Interaction for Submarine Pipelines, 2017;

26 D. J. White, Z. J. Westgate, J-C Ballard, C. De Brier, M. F. Bransby, Best Practice Geotechnical Characterisation and Pipe-soil Interaction Analysis for HPHT Pipeline Design. Proc. Offshore Technology Conference, OTC, Houston, 2015, Paper no. 26026;

27 G. E. P. Box; K. B. Wilson, On the Experimental Attainment of Optimum Conditions, Journal of the Royal Statistical Society: Series B. 13 (1): 1–45, 1951;

28 R. H. Myers, D.C. Montgomery, C. M. Anderson-Cook, Response Surface Methodology: Process and Product Optimization using Designed Experiments, USA: Hoboken, N.J. : Wiley, 2009;

29 G. G. Wang, Adaptive Response Surface Method Using Inherited Latin Hypercube Design Ppoints. Trans-Am Soc Mech Eng J Mech Design, 125(2):210–220, 2003;

30 D. Shepard, A two-dimensional interpolation function for irregularly-spaced data, Proceedings of the 1968 ACM National Conference. pp. 517–524, 1968;

31 Standard, DNV-GL-ST-F101, Submarine Pipeline Systems, 2017;

32 Recommended Practice, DNV-RP-F105, Free Spanning Pipelines, 2006;

33 ASME B36.10M, Welded and Seamless Wrought Steel Pipe, 2018;

34 Recommended Practice, DNV-RP-F110, Global Buckling of Submarine Pipelines, 2007;

35 Z. Hong, W. Liu, Modelling the vertical lifting deformation for a deep-water pipeline laid on a sleeper, Ocean Engineering, 199 (2020) 107042;

36 Z. Wang, Z. Chen, H. Liu, Z. Zhang, Numerical study on lateral buckling of pipelines with imperfection and sleeper, Applied Ocean Research, 68 (2017) 103–113.